J. Fluid Mech. (1997), *vol.* 346, *pp.* 49–76. Printed in the United Kingdom

© 1997 Cambridge University Press

Vorticity filaments in two-dimensional turbulence: creation, stability and effect

By N. K.-R. KEVLAHAN AND M. FARGE
LMD-CNRS, Ecole Normale Supérieure, 24, rue Lhomond, 75231 Paris Cedex 05, France

(Received 6 February 1997)

Vorticity filaments† are characteristic structures of two-dimensional turbulence. The formation, persistence and effect of vorticity filaments are examined using a high-resolution direct numerical simulation (DNS) of the merging of two positive Gaussian vortices pushed together by a weaker negative vortex. Many intense spiral vorticity filaments are created during this interaction and it is shown using a wavelet packet decomposition that, as has been suggested, the coherent vortex stabilizes the filaments. This result is confirmed by a linear stability analysis at the edge of the vortex and by a calculation of the straining induced by the spiral structure of the filament in the vortex core. The time-averaged energy spectra for simulations using hyper-viscosity and Newtonian viscosity have slopes of -3 and -4 respectively. Apart from a much higher effective Reynolds number (which accounts for the difference in energy spectra), the hyper-viscous simulation has the same dynamics as the Newtonian viscosity simulation. A wavelet packet decomposition of the hyper-viscous simulation reveals that after the merger the energy spectra of the filamentary and coherent parts of the vorticity field have slopes of -2 and -6 respectively. An asymptotic analysis and DNS for weak external strain shows that a circular filament at a distance R from the vortex centre always reduces the deformation of a Lamb's (Gaussian) vortex in the region $r \geqslant R$. In the region $r < R$ the deformation is also reduced provided the filament is intense and is in the vortex core, otherwise the filament may slightly increase the deformation. The results presented here should be useful for modelling the coherent and incoherent parts of two-dimensional turbulent flows.

1. Introduction

High-resolution direct numerical simulations (DNS) have shown that two-dimensional turbulent flows always produce coherent vortices from an initially unorganized vorticity field (e.g. Fornberg 1977; Basdevant *et al.* 1981; McWilliams 1984). However, once a sufficient number of vortices have formed the main interactions are vortex mergers and pairings (i.e. the formation of a dipolar structure made up of opposite-signed vortices). The strong shearing associated with the vortex mergers produces intense filaments of vorticity; however these filaments, unlike the initial unorganized vorticity field, are usually stable and do not roll up to create new vortices via the Kelvin–Helmholtz instability. Vorticity filaments are thus a characteristic feature of fully developed two-dimensional turbulent flows.

† We use the term 'filament' to refer exclusively to the thread-like structures observed in two-dimensional turbulence; they should not be confused with the vortex tubes of three-dimensional turbulence. This terminology is discussed in Appendix A.

In fact, the filaments created during vortex mergers must be stabilized in order to be consistent with the observed dynamics of two-dimensional turbulence. If the filaments were unstable they would roll up and create large numbers of new smaller vortices. The process of merger would then continue at the smaller scale of the new vortices, and with the same result: more, even smaller, vortices would be created at each generation 'and so on to viscosity'. However, we know that energy is not (on average) transferred to smaller scales in two-dimensional turbulence, and that the size of vortices increases and their number decreases with time. Therefore the filaments must be externally stabilized so they do not create new vortices. The fact that filaments are always associated with coherent vortices (since they are created during the merger or tearing of such vortices) suggests that it is the coherent vortices which stabilize the filaments.

In order to understand two-dimensional turbulence it is therefore important to know precisely how the coherent vortices stabilize the filaments. Dritschel (1989) has shown that a sufficiently strong adverse shear can stabilize a two-dimensional vortex strip, and Dritschel *et al.* (1991) showed that straining can also stabilize a two-dimensional vortex strip. These results suggest possible mechanisms for stabilizing the filaments, but it is not clear which mechanisms are actually effective in real flows, nor where and how they are effective. Finally, although it is reasonable to suppose that the coherent vortices are the source of the stabilization this has not been demonstrated conclusively.

Even if the filaments are stable, they may still have an effect on the dynamics or spectral properties of the flow. For example, Gilbert (1988) showed that a spiral vorticity filament can produce a power-law energy spectrum with non-integer slopes. A spiral vorticity filament may even produce an energy spectrum very similar to that measured in two-dimensional turbulent flows (Gilbert 1988; Vassilicos & Hunt 1991). Perhaps it is the vorticity filaments that determine the slope of the turbulence energy spectrum. At larger times the filaments formed during a vortex merger tend to be distributed as a sequence of approximately circular rings around the coherent vortex. Does this intense shear layer at the edge of the coherent vortex shield it from the strain field of the neighbouring vortices, or does it enhance this strain? If such shielding (or amplification) could occur it would increase (decrease) the critical distance for vortex merger (Dritschel & Waugh 1992) and significantly affect the dynamics.

In order to successfully model a two-dimensional turbulent flow it is essential to understand the role of vorticity filaments. If the filaments remain passive (apart from viscous decay) they could be modelled quite simply. Should the model retain the filamentary geometry at all, or merely replace it by a Gaussian noise with the same energy spectrum? If the filaments have no effect on the flow dynamics this may be a good model, but if the filaments change the effect of external strain on the coherent vortices a more sophisticated model may be required.

The questions raised here are investigated by analysing a high-resolution DNS of the merger of two identical positive Gaussian vortices pushed together by a smaller negative vortex. This is a very strong interaction that produces many intense vorticity filaments. Such mergers are the main interactions of fully developed two-dimensional turbulence and should contain its basic dynamics and kinematics. The results of the simulation are presented in §2, and quantities such as the geometry of the flow and evolution of the Fourier energy spectrum are analysed. In addition, simulations are done using both hyper-viscosity and Newtonian viscosity, and the results are compared in order to determine whether hyper-viscosity introduces any spurious

effects (as has been suggested by Farge, Holschneider & Colonna 1990; Jiménez 1994 and Yao, Zabusky & Dritschel 1995).

The stabilizing effect of the coherent vortices on the filaments is then demonstrated in section §3 using a wavelet packet decomposition of the vorticity field introduced by Farge *et al.* (1992) and further DNS. The stabilizing effect of the coherent vortices is explained analytically using both a linear stability analysis based on that of Dritschel (1989), and a calculation of spiral straining in the vortex core.

Finally, in §4 the effect of vorticity filaments on the dynamics of a coherent vortex in the weak strain field produced by other distant vortices is examined. We use the asymptotic approach introduced by Ting & Tung (1965) and developed by Jiménez, Moffatt & Vasco (1996) to calculate the deformation of a Gaussian vortex surrounded by a circular vorticity filament, and compare it to the deformation of the vortex alone. This calculation shows that in certain cases the deformation can be reduced by the presence of the vorticity filament, and in others the deformation may be increased slightly.

The results are summarized in §5 and the implications for modelling two-dimensional turbulence are noted. In particular, the possible contribution of vorticity filaments to the overall properties of a two-dimensional turbulent flow are discussed. These investigations should give a fairly complete picture of the creation, stability and effect of vorticity filaments in two-dimensional turbulence.

2. Simulation of vortex merger

2.1. *Initial conditions*

Vorticity filaments form in two-dimensional turbulence during the merger of coherent vortices due to the strong shear forces that develop during the interaction. These forces pull some of the vorticity out into long, narrow strips of intense vorticity which are usually spiral in shape. It is these narrow strips of intense vorticity that we mean when referring to 'vorticity filaments'. In order to study the formation and subsequent evolution of vorticity filaments we will simplify the turbulent flow to a particular system of three vortices in a strong interaction that leads to a fast vortex merging. This is a good approximation to the situation in fully developed two-dimensional turbulence when the coherent vortices have emerged.

The particular initial condition we choose is a triangular arrangement of two positive vortices, π units apart, and one negative vortex, $\pi/(2\sqrt{2})$ above the right-hand vortex, as shown in figure 1. The vortices all have Gaussian profiles $\omega(r,0) = \Gamma/(\pi r_0^2)\exp(-r^2/r_0^2)$, with the circulation $\Gamma = 1$ for the positive vortices and $\Gamma = -1/2$ for the negative vortex, and the vortex radius $r_0 = 1/\pi$. Inviscid point vortices in this arrangement collapse to the same point in a finite time $3/8\pi^3\sqrt{2}$ (Novikov & Sedov 1979; Aref 1979; Marchioro & Pulvirenti 1994, pp. 139–140) and thus this arrangement ensures a rapid merger.

These initial conditions are quite specific, but the general dynamics of the interaction should not depend critically on the precise arrangement of the vortices. In fully developed two-dimensional turbulent flows the chance of vortex merging increases with the density of vortices; here with only three vortices we need this specific configuration to ensure a rapid merger. The negative vortex effectively replaces the mean field which pushes vortices together and induces merging. In fact the configuration we have chosen should be fairly realistic since in practice mergers are often caused by a fast-moving dipole running into another vortex – this is modelled

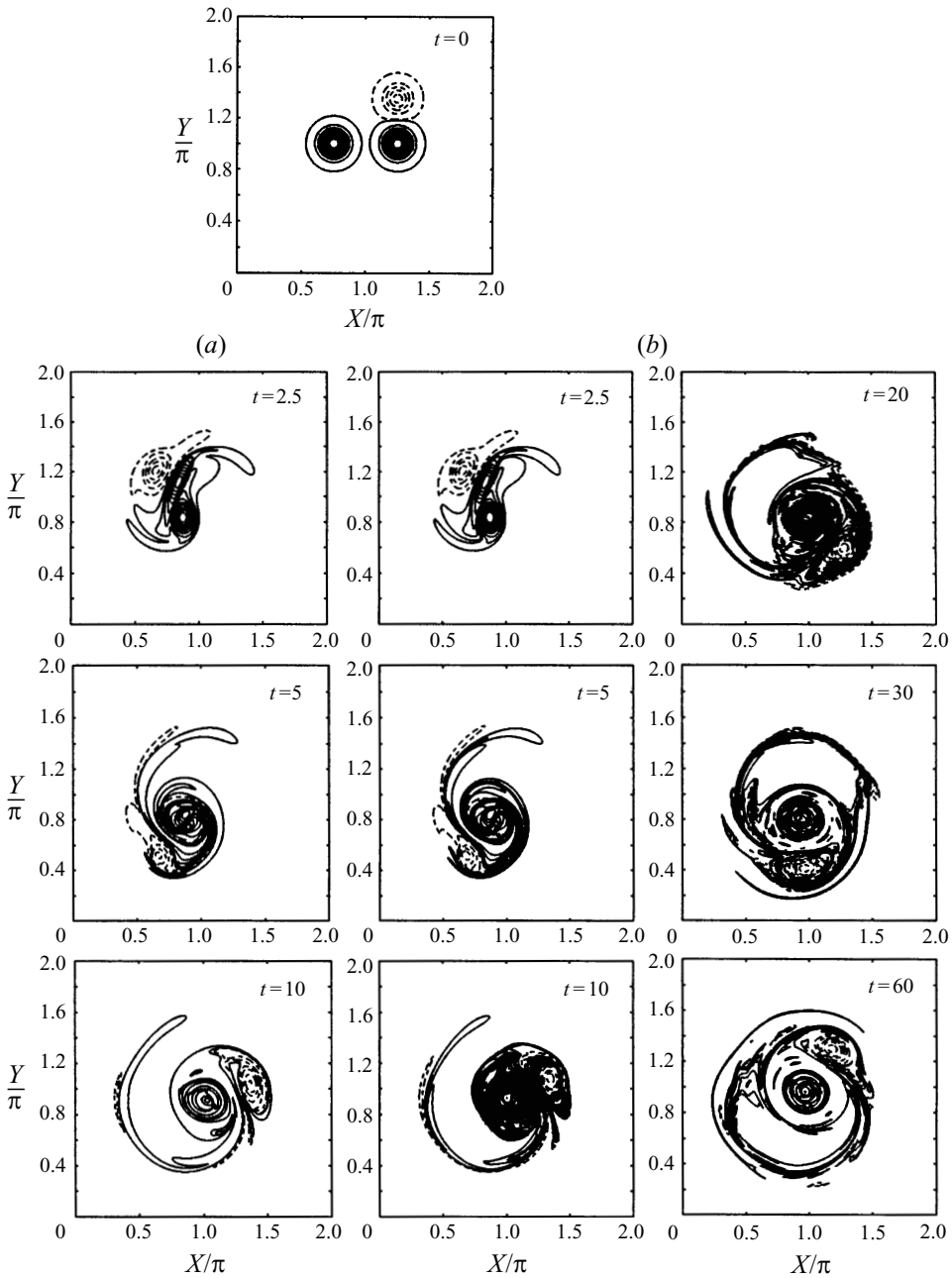

FIGURE 1. Vortex merger in physical space: —, 10 contours of vorticity equally spaced between $(\pi/100, \pi)$; – – –, 10 equally spaced contours between $(-\pi/100, -\pi)$. Time is measured in terms of the initial turn-over time of one of the positive vortices. (*a*) Newtonian viscosity simulation, (*b*) hyper-viscous $p = 8$ simulation.

by the three-vortex initial condition. Recent work by Dritschel & Zabusky (1996) has also shown that the three-vortex interaction (where one vortex is of the opposite sign) is the only significant interaction of a dilute distribution of vortices on a sphere. Indeed, figure 2(*a*) of Dritschel & Zabusky (1996) shows an interaction very similar

Resolution	Viscosity	Re_Γ	Δt	Maximum time
256^2	$\nu = 1 \times 10^{-4}$	10^4	1.25×10^{-3}	20
256^2	$\nu_{16} = 5.9 \times 10^{-30}$	—	1.25×10^{-3}	75
1024^2	$\nu = 5 \times 10^{-5}$	2×10^4	6.25×10^{-4}	60
1024^2	$\nu_{16} = 1.2 \times 10^{-39}$	—	6.25×10^{-4}	60

TABLE 1. Parameters for the DNS performed. The Reynolds number $Re_\Gamma = \Gamma/\nu$ where Γ is the initial circulation of a positive vortex, and the times have been normalized by the initial turn-over time T of a positive vortex based on the initial maximum vorticity ω_0 ($T = 4\pi/\omega_0 = 4$). Δt is the time step. Note that Reynolds numbers cannot be accurately defined for the hyper-viscous simulations.

to the one considered here. For all the above reasons, the three-vortex interaction is a good choice. Rapid collapse interactions of this type have been studied recently by Vosbeek *et al.* (1997).

The vorticity

$$\omega = -\nabla^2\psi, \tag{2.1}$$

where ψ is the stream function, is found by numerically solving the two-dimensional vorticity equation

$$\frac{\partial\omega}{\partial t} - J(\psi,\omega) = \nu\nabla^2\omega, \tag{2.2}$$

where ν is the kinematic (Newtonian) viscosity and the Jacobian $J(\psi,\omega)$ is defined as

$$J(\psi,\omega) = \frac{\partial\psi}{\partial x}\frac{\partial\omega}{\partial y} - \frac{\partial\psi}{\partial y}\frac{\partial\omega}{\partial x}. \tag{2.3}$$

The equations are solved using a pseudo-spectral code with an Adams–Bashforth time step developed by Basdevant (Basdevant *et al.* 1981). In addition to the usual vorticity equation (2.2) we also made simulations using hyper-viscosity where the dissipation term $\nu\nabla^2\omega$ is replaced by a hyper-dissipation term $-\nu_{2p}\nabla^{2p}\omega$ (first proposed by Basdevant *et al.* 1981). Hyper-dissipation compresses the dissipation range into a smaller range of scales and thus increases the inertial range thereby approximating a higher-Reynolds-number flow. By doing simulations using hyper-viscous dissipation we can simulate some aspects of very high-Reynolds-number flows, but we will compare this simulation with the Newtonian viscosity simulations to ensure that no important spurious effects are introduced. The simulations performed are summarized in table 1. The results presented in the following sections are all obtained from the high-resolution 1024^2 simulations.

2.2. *Results*

2.2.1. *Physical space representation*

The two positive vortices merge quickly, creating tightly wrapped spirals of intense vorticity (the filaments). The negative vortex is deformed, but remains relatively passive and does not merge with the two positive vortices (in contrast to the case of inviscid point vortices discussed by Marchioro & Pulvirenti 1994 where all three vortices reach the same point after a finite time). However, a small amount of negative vorticity is pulled out and wrapped around the two positive vortices while they are merging. This leads to a very large vorticity gradient in the direction perpendicular to the filaments. In fact, the filaments are very smooth along their axes of elongation and

quasi-singular in the perpendicular direction. The portion of the spiral in the vortex core rapidly blends into the Gaussian vorticity profile, but well-defined filaments persist at the edge of the new coherent vortex. The 'long time' configuration is an approximately Gaussian coherent vortex to which vorticity bumps or 'kinks' have been added, surrounded by a ring of approximately circular filaments at the edge of the vortex core. Note that some vorticity is ejected as a filament far from the vortex core, but most filaments are tightly wrapped around the core. This is due to the fact that in this configuration there are no external vortices present which could pull the vorticity filaments away from the region where they formed. The merger is shown for Newtonian viscosity in figure 1(*a*) and for hyper-viscosity in figure 1(*b*).

The new vortex contains roughly half the enstrophy of the initial positive vortices, the rest having been lost to filaments and dissipation. This loss is much higher than the range observed by Waugh (1992) in contour surgery simulations of symmetric vortex merger in the absence of external forcing. It appears that the presence of the negative vortex reduces the efficiency of the merger (the proportion of enstrophy in the new vortex compared to the total enstrophy of the initial vortices) and slows the increase in the length scale of the new vortex (in this case there is virtually no increase in the length scale of the coherent vortex). In fully turbulent flows the interactions generally involve several vortices, and thus the efficiency is likely to be closer to that observed here than to that observed by Waugh (1992).

A cut through the vortices (figure 2) shows that the filaments in the core decay quickly due to dissipation, but leave 'kinks' in the vorticity profile. After the merger is complete and the core filaments have decayed the equilibrium profile is the same Gaussian as the initial positive vortices, with the kinks superimposed, and surrounded by a ring of weak vorticity filaments. The negative vortex, on the other hand, has had the weaker vorticity at its edge stripped away, which has steepened its vorticity profile (vorticity stripping has been investigated by Mariotti, Legras & Dritschel 1994). The vorticity filaments never show any signs of developing instabilities.

A comparison of the Newtonian viscosity and hyper-viscous vorticity contours (figures 1*a* and *b*) and cuts (figures 2*a* and *b*) shows that, although the hyper-viscous simulations produce stronger gradients that decay more slowly, the shape of the vortices and the position of vorticity filaments are identical in both simulations. The only unphysical feature of the hyper-viscous simulations is that the maximum vorticity of the filaments slightly surpasses the initial maximum (by about 2%) for a short period of time; this is a well-known problem (Jiménez 1994). From this comparison it is seems likely that the hyper-viscous simulation is a good approximation to the true high-Reynolds-number flow (e.g. stronger gradients and slower decay). Thus we should be able to use the hyper-viscous simulations as a guide to the behaviour of the equivalent very high-Reynolds-number flow. This is important because many features of two-dimensional turbulence (such as scaling in the energy spectrum) only become clear at higher Reynolds numbers.

Our results contrast with those of Yao *et al.* (1995) who investigated the effect of hyper-dissipation on the simulation of the interaction of two positive vortices of unequal sizes. Yao *et al.* found that hyper-dissipation caused a large overshoot of the maximum vorticity of up to 30%, although the agreement between Newtonian viscosity, hyper-viscosity and contour surgery simulations was good until dissipation became important. The hyper-dissipation simulation was also more smoothing than the contour surgery simulation, but in this case it is not clear which simulation is actually closest to true high-Reynolds-number dynamics. There are a number of differences that could explain why we find that hyper-dissipation produces no

Structure	Singularity	$2p$
Point vortex	ω	1
Circular ring (zero width)	ω	2
Circular ring (rectangular cross-section)	$\mathrm{d}\omega/\mathrm{d}r$	4
Circular ring (triangular cross-section)	$\mathrm{d}^2\omega/\mathrm{d}r^2$	6

TABLE 2. Energy spectra $E(k) \propto k^{-2p}$ at small scales associated with various types of singular vortical structures ($E(k) \propto \hat{\omega}(k)^2/k$).

important spurious effects. The first, and most important, difference is that we consider vortices with a smooth Gaussian profile, while Yao *et al.* consider vortex patches with a completely flat centre and high-gradient sides. The Gaussian vortex is a solution of the Navier–Stokes equations, while the vortex patch is clearly not. The initial condition chosen by Yao *et al.* is thus not well-suited to a simulation of the Navier–Stokes equations, but is appropriate for the contour surgery method. Secondly, we consider the interactions of vortices of the same size. Thirdly, we use a ∇^{16} hyper-dissipation operator, while Yao *et al.* use a ∇^4 operator. Finally, our high-resolution simulation completely resolves the fine-scale structure of the flow, which may not be the case for the 512^2 simulation of Yao *et al.*

2.2.2. *Fourier space representation*

High-resolution DNS of quasi-equilibrium two-dimensional turbulence usually has an energy spectrum† of about $E(k) \propto k^{-3.5}$ in the inertial range (Legras, Santangelo & Benzi 1988), but depending on the forcing the slope may be anywhere in the range $(-3, -6)$. The slope -3.5 is mid-way between the theoretical value of -4 proposed by Saffman (1971) assuming that the spectrum is dominated by discontinuities of vorticity, and the value of -3 proposed by Kraichnan (1967) and Batchelor (1969) for statistically homogeneous and isotropic two-dimensional turbulence based on the notion of a local cascade of enstrophy from the forcing scale to the dissipation scale. By examining the energy spectrum of the vortex merger and comparing it to the physical space structure we will try to understand the reasons for this discrepancy, although we are aware that we are not actually dealing with quasi-equilibrium turbulence.

Since vorticity filaments are a characteristic feature of the interaction it is useful to recall the energy spectra associated with various simple filamentary structures. The energy spectrum slopes as the scale goes to zero of various types of simple singular vortex structures are shown in table 2. At coarser scales the Fourier transform will 'see' a more singular structure, e.g. the energy spectrum of a ring of finite width has slopes of -4, -2 and -1 at successively larger scales. As Vassilicos & Hunt (1991) pointed out, a non-trivial geometry (e.g. an accumulating spiral with a Kolmogorov capacity $D'_K > 1$) can make a structure effectively more singular and thus decrease the slope of the energy spectrum.

Gilbert (1988) showed that the energy spectrum of the spiral created when a weak patch of vorticity winds around a strong vortex has a non-integer slope given by

$$E(k) \propto k^{-4+(s-1)/(s+1)}, \tag{2.4}$$

† One should be very cautious when making a statistical interpretation of energy spectra obtained from numerical experiments on turbulent flows (see Appendix B).

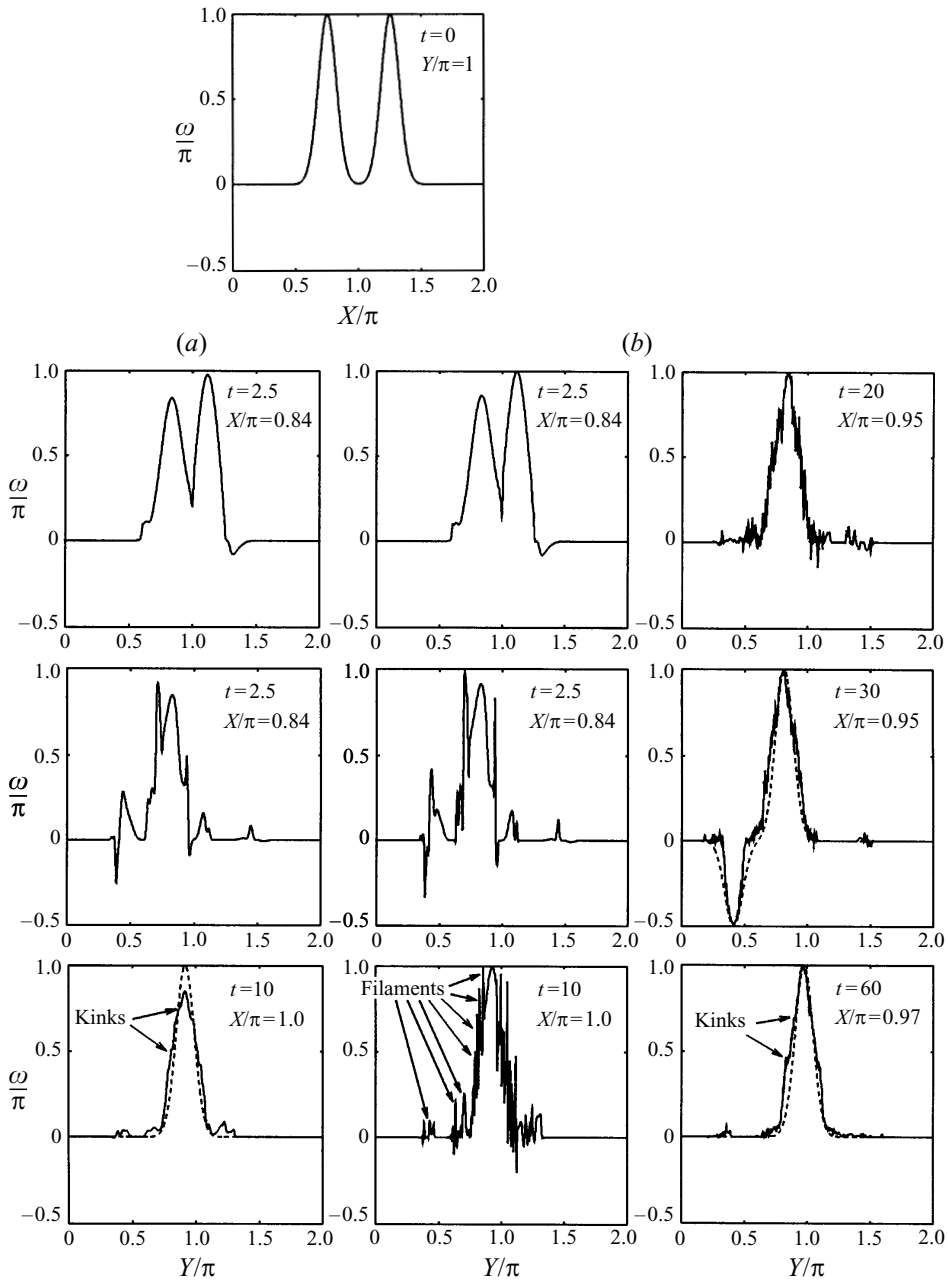

FIGURE 2. Cut through the vorticity field, – – – is the original Gaussian vorticity profile. (*a*) Newtonian viscosity, (*b*) hyper-viscosity.

where $\pi\Gamma/r^{-s}$ is the angular velocity of the vortex of strength Γ. For a point vortex, or the far field of a Gaussian vortex, $s = 2$ and thus $E(k) \propto k^{-3.67}$, similar to values measured in DNS. Thus Gilbert proposed that spiral vorticity filaments may provide a bridge between the theories of Saffman and Batchelor–Kraichnan.

In this section we examine the evolution of the energy spectrum of the three-vortex interaction to see how the results compare to the predictions of Gilbert (1988) and

to the results from fully turbulent DNS. When comparing the results here with the predictions of Gilbert (1988) it is important to bear in mind that he assumed that the spiral vorticity was weak (and therefore passive), and that there is no external strain. In our case, the merging vortices are of equal strength, and the negative vortex provides an external strain that pushes the positive vortices together.

The Fourier energy spectrum at various times for the hyper-viscous and Newtonian viscosity simulations are shown in figure 3 and the evolution of the slope $2p$ of the energy spectrum $E(k) \propto k^{-2p}$ is shown in figure 4. Two power-law ranges develop early on in the interaction: a large well-defined relatively shallow slope at intermediate scales, and a smaller less well-defined steeper one at smaller scales. Both slopes quickly decrease to a minimum at the time of merger (about $t = 5.3$) and then slowly increase again. The hyper-viscous simulation, as expected, has shallower slopes (associated with stronger gradients) and decays very slowly to a quasi-equilibrium of about -3. The value of -3 is the limit of Gilbert's result (2.4) for vortices with very strong shear ($s \gg 1$) or space-filling filaments. This may mean that our forced interaction is equivalent to the passive wrapping of a vortex patch around a vortex with very strong shear. In fact we observe that half of the enstrophy of the two positive vortices is transformed from coherent structures to vorticity filaments.

We have checked that these spectral results are not specific to this particular merger interaction by examining the merging of two unequal vortices of the same sign. The larger vortex has the size $R = 1$, the smaller has the size $R = 0.7$, they are initially separated by a distance $r = 2.2$ and they have equal maximum vorticity. This interaction also develops an intense spiral in physical space and a power-law energy spectrum: the slope of the energy spectrum becomes as shallow as -1.5 at the time of merger, before reaching the quasi-equilibrium value of -3. Note that the slope -1.5 indicates that the filaments have a non-trivial accumulating spiral structure and that they dominate the energy spectrum (see Vassilicos & Hunt 1991 for a discussion of accumulating spiral structures). These results suggest that the generation of power-law energy spectra and accumulating spiral structures is a fairly general characteristic of vortex merger in two dimensions. In particular, the long-term k^{-3} spectrum appears to be generic.

It would be useful to directly calculate the energy spectrum due to the filaments alone, to see if there is any evidence of non-trivial (i.e. the wrapping becomes infinitely tight, or 'accumulating', at the centre) spiral structure. We have therefore divided the hyper-viscous vorticity field at $t = 10$ into filamentary and coherent vortex parts using a wavelet packet algorithm developed by Farge *et al.* (1992). We first project the vorticity field onto a wavelet packet basis and plot the cumulative energy contained in the wavelet packet modes (see figure 5*a*). The division between the filamentary and coherent vortex parts of the flow occurs at the second change in slope on the plot in figure 5(*a*), the corresponding percentage is found by fitting straight lines to the straight sections and finding the intersection. This calculation shows that the largest 31 modes containing 83% of the enstrophy correspond to the coherent vortices, while the remaining 1 048 545 modes which contain 17% of the enstrophy correspond to the filamentary part of the vorticity field. It was checked that 83% is enough to just separate the filamentary and coherent parts of the flow. Figure 5(*b–d*) shows cross-sections of the total vorticity field, the coherent part and the filamentary part. The results of this decomposition are presented in figure 6 and show that this method clearly separates spiral filaments from the vortices (no filamentary structure remains in the vortex core).

Figure 6(*c*) shows that the filaments have an intermediate-range energy spectrum

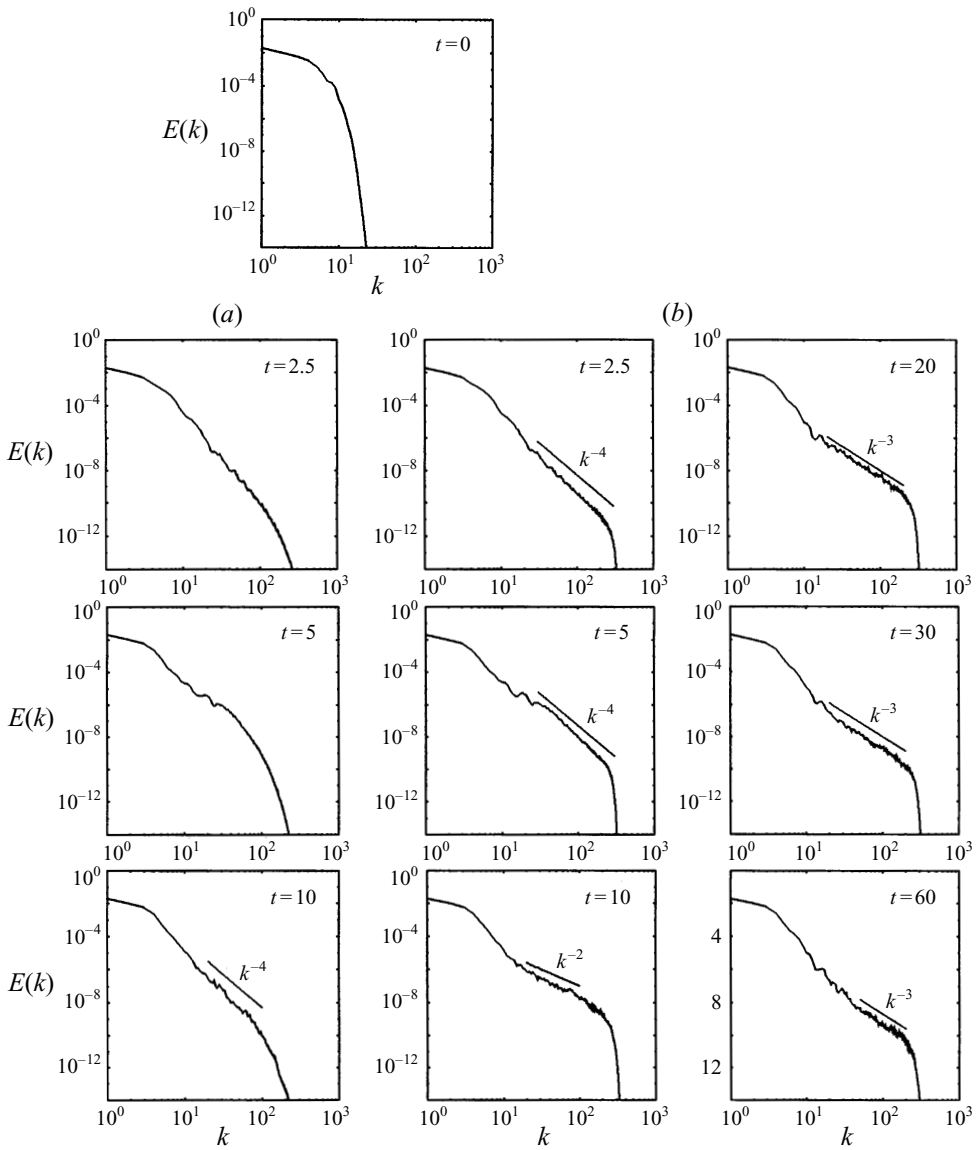

FIGURE 3. Fourier energy spectrum of the simulations. (*a*) Newtonian viscosity, (*b*) hyper-viscosity.

with a power law like k^{-2}, while the vortical part has a power law like k^{-6} which confirms previous observations (Farge *et al.* 1992). Note that the power-law range of the filamentary part extends to large scales, while the power-law range of the coherent part extends to small scales. This indicates that both filamentary and coherent parts are multi-scale and cannot be separated by a simple Fourier high-pass filter. The small difference between the spectra of the total field and that of the filamentary part alone indicates that the filaments control the overall spectrum of the flow in the intermediate and small scales.

Figure 6(*g*) shows that at $t = 30$ all three fields have an energy spectrum like k^{-3} at intermediate scales. At the same time figure 2(*b*) shows that the spiky filaments have decayed to kinks, and thus it is the combination of the kinks and the Gaussian core

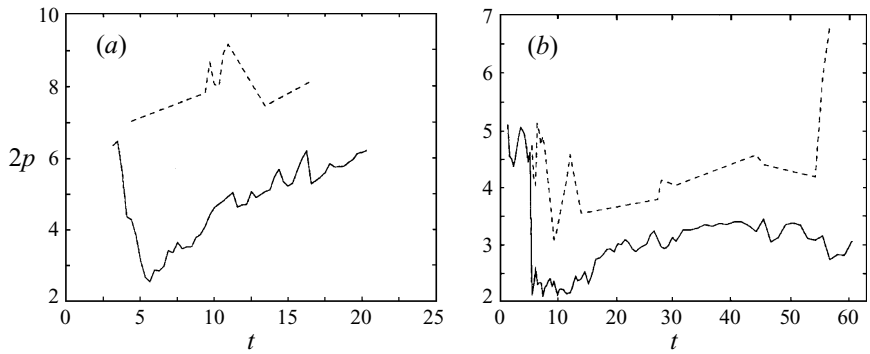

FIGURE 4. Evolution of energy spectrum slope $2p$; the solid and dashed lines indicate slopes in the well-defined intermediate-scale and poorly defined small-scale ranges respectively. (*a*) Newtonian viscosity simulation, (*b*) hyper-viscosity simulation.

which produce the k^{-3} spectrum. This may be understood by noting that the kinks are discontinuities in the slope of the vorticity which gives a k^{-6} spectrum at small scales and a k^{-4} spectrum at intermediate scales; the accumulating spiral structure can then reduce this slope further from -4 to -3. It is interesting to note that although all filaments were removed from the coherent field at $t = 10$, by $t = 30$ enough irregularities had formed to change the slope of the energy spectrum from -6 to -3. This suggests that the -3 slope is an extremely robust property of two-dimensional vortical flows.

A good indication of the energy spectrum of a fully turbulent flow may be obtained by averaging the energy spectrum of the merger over the period of the interaction. This reproduces the spectrum of a turbulent flow containing many merging events at various stages. The plots of the time-averaged energy spectra for the two simulations are shown in figure 7. The hyper-viscous simulation has a large power-law range of about k^{-3}, while the Newtonian viscosity simulation has a smaller power-law range of k^{-4}. These time-averaged spectra are compatible with results from DNS of two-dimensional turbulence which suggests that the complete merging interaction is a fundamental interaction of two-dimensional turbulence.

Recently Nielsen *et al.* (1996) did a similar simultaneous analysis of a vortex merger in physical and Fourier space. They considered the merger of two identical vortices using hyper-viscous DNS and found that the interaction creates an energy spectrum with a slope of about -4. This slope is slightly steeper than the slope of -2 to -3 we have found, probably because the three-vortex interaction creates much stronger gradients and tighter spiral wrapping of vorticity. Nielsen *et al.* also attempted to separate out the structures responsible for this spectrum by taking a Fourier high-pass filter of the field. They concluded that the -4 slope is associated with the "distorted vortex boundary". As noted earlier, a high-pass filter cannot accurately or completely separate the two parts of the field since they are both multi-scale. However, in general our results agree with those of Nielsen *et al.* since we find that the power-law intermediate-range energy spectrum of the total field is associated with spiral filaments of intense vorticity. Our analysis definitely confirms the main result of Nielsen *et al.* that a collection of coherent structures of all sizes is not required to generate an inertial-range energy spectrum typical of two-dimensional turbulence. Farge & Holschneider (1991) have proposed a different model for the vortices of two-dimensional turbulence: a cusp, which is also able to reproduce a

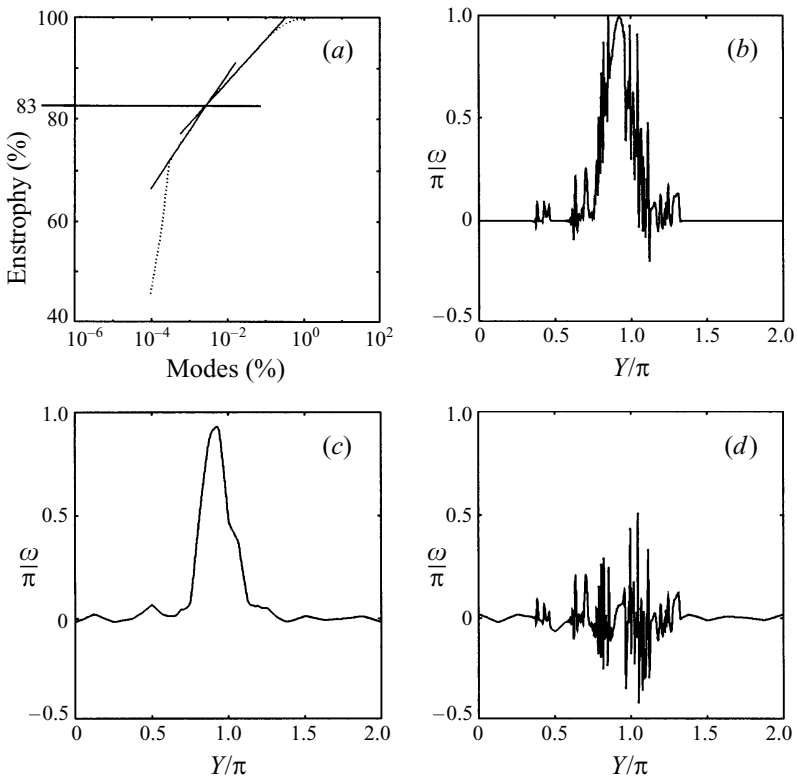

FIGURE 5. (*a*) Cumulative energy contained in the wavelet packet coefficients at $t = 10$. The coherent vortices are represented by those modes below the second kink, and the remaining modes define the filaments (straight lines have been fitted). (*b*) Cross-section of the vorticity field at $t = 10$, $x/\pi = 1$. (*c*) Coherent part of the vorticity field, note that filaments have been removed completely. (*d*) Filamentary part of the vorticity field.

power-law energy spectrum without resorting to a hierarchy of vortices of different sizes.

3. Stability of vorticity filaments

In the previous Section we saw that the vorticity filaments created during the merging interaction show no signs of instability, neither in the hyper-viscous simulation, nor in the Newtonian viscosity simulation. Dritschel (1989) has suggested that the coherent vortices may stabilize the vorticity filaments in two-dimensional turbulence. We now test this theory directly by separating the vorticity field into filamentary and coherent parts as described in §2.2.2 and restarting the simulation with these three fields (total, coherent, filamentary) as separate initial conditions.

Figure 6 clearly demonstrates that it is the coherent vortex that stabilizes the filaments: the total field shows no signs of instability; however, when the vorticity field contains only filaments they are quickly destabilized by the Kelvin–Helmholtz instability and form many new coherent vortices. It is interesting to note that by $t = 30$ all three fields have developed the same energy spectrum: the cascade spectrum k^{-3}. Thus the filaments alone have created a kind of two-dimensional turbulence!

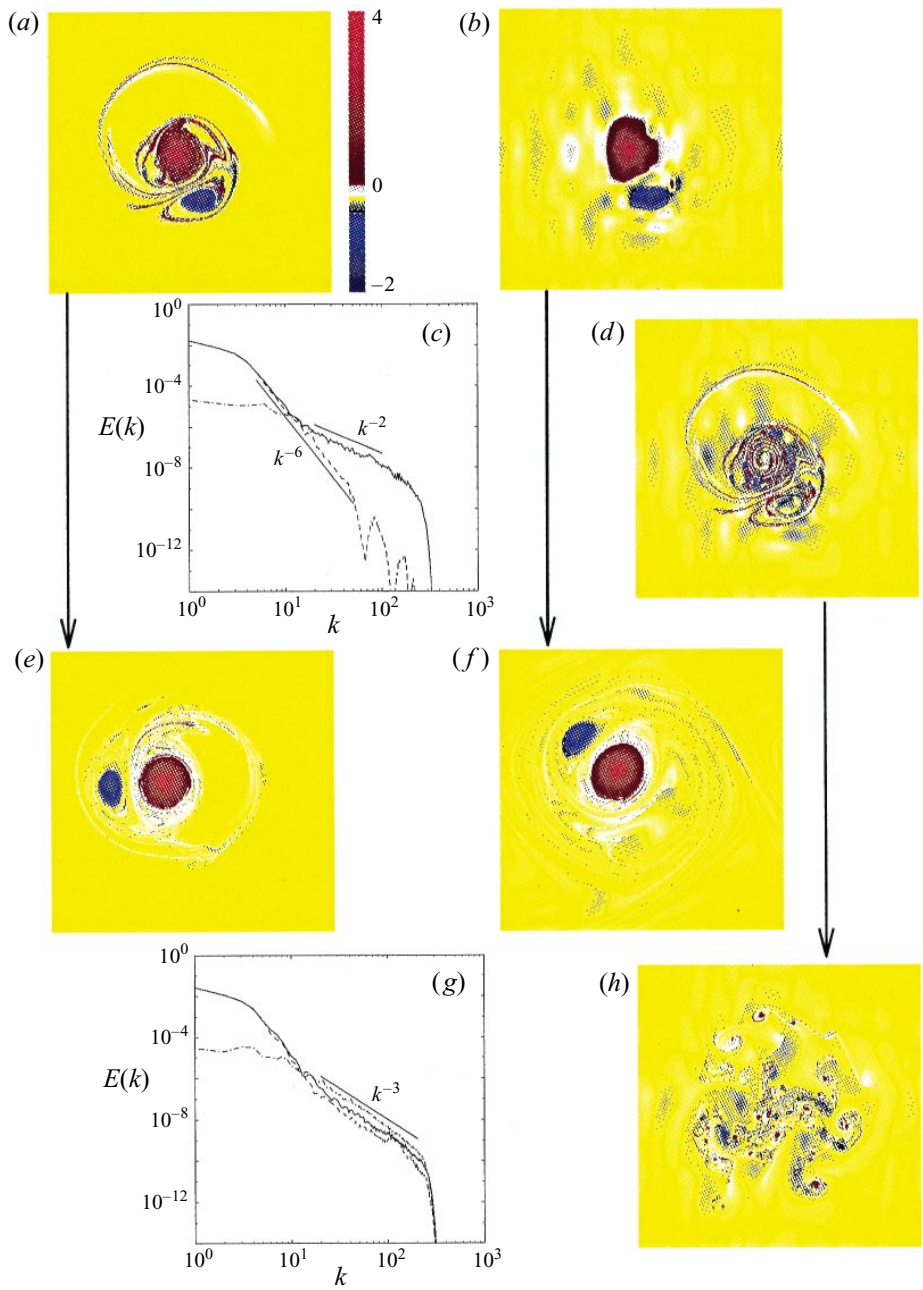

FIGURE 6. Dynamical analysis of coherent structures and incoherent background flow. (*a*) Total vorticity at $t = 10$ computed with a resolution 1024^2. (*b*) Vorticity corresponding to the coherent vortices alone at $t = 10$. They are made up of 31 strong wavelet packet coefficients which contain 83% of the total enstrophy. (*c*) Energy spectra at $t = 10$: —, the total energy spectrum; – – –, the coherent vortices energy spectrum; – · –, the filament energy spectrum. (*d*) Vorticity corresponding to the filaments alone at $t = 10$. They are made up of 1 048 545 weak wavelet packet coefficients which contain 17% of the total enstrophy. (*e*) Integration of the total vorticity up to $t = 30$. (*f*) Integration of the coherent vortices alone up to $t = 30$. (*g*) Energy spectra at $t = 30$: —, the total energy spectrum; – – –, the coherent vortices energy spectrum; – · –, the filament energy spectrum. (*h*) Integration of the filaments alone up to $t = 30$.

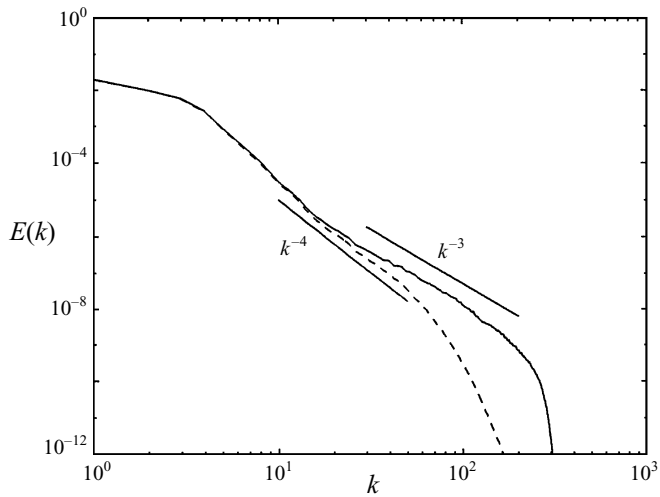

FIGURE 7. Time-averaged energy spectra: —, hyper-viscosity simulation; – – –, Newtonian viscosity simulation.

We have demonstrated that the vortex stabilizes the filaments, but we have not yet explained how it does it. Two mechanisms have been suggested: adverse shear (Dritschel 1989) and straining (Dritschel *et al.* 1991). We will first consider the adverse shear mechanism.

3.1. *Adverse shear*

Following Dritschel's (1989) approach we do a linear stability analysis of a circular strip of vorticity (rectangular cross-section), but substitute a Gaussian central vortex for the circular vortex patch he considered. We consider a Gaussian vortex to be a good model of a coherent vortex (as suggested by McWilliams 1984) because when coherent structures are widely separated they relax to the Gaussian shape under the effect of diffusion (the nonlinear Jacobian terms of the Navier–Stokes equations are zero in this case). Consider the basic state defined by a ring of uniform vorticity ω bounded inside by the circle $r = a$ and outside by the circle $r = b$. Adverse shear is introduced by placing a Gaussian vortex $\omega(r) = \Gamma/(\pi r_0^2)\exp(-r^2/r_0^2)$, of circulation Γ and radius r_0, at the origin.

The net rotation rate of the system (reference frame, Gaussian vortex and strip) is

$$\Omega + \tfrac{1}{2}\omega\left(1 - \frac{a^2}{r^2}\right) + \frac{\Gamma}{2\pi r^2}\left(1 - \exp(-r^2/r_0^2)\right), \tag{3.1}$$

where Ω is the rotation rate of the reference frame, the second term is the contribution from the strip, and the third term is the contribution from the Gaussian vortex. The rotation rate of the reference frame is chosen so that the two edges of the strip, in equilibrium, rotate at the same rate, but in opposite directions. Therefore we must have

$$\Omega + 0 + \frac{\Gamma}{2\pi a^2}\left(1 - \exp(-a^2/r_0^2)\right) = -\Omega - \tfrac{1}{2}\omega\left(1 - \frac{a^2}{b^2}\right) - \frac{\Gamma}{2\pi b^2}\left(1 - \exp(-b^2/r_0^2)\right), \tag{3.2}$$

and thus

$$\Omega = -\tfrac{1}{4}\omega\left(\left[(1+\Lambda) - \frac{a^2}{b^2}(1-\Lambda)\right] - \Lambda\left[\exp(-a^2/r_0^2) + \frac{a^2}{b^2}\exp(-b^2/r_0^2)\right]\right), \tag{3.3}$$

where $\Lambda = \Gamma/(\pi a^2\omega)$ is the dimensionless adverse shear.

Linear stability is determined by adding disturbances of the form

$$\eta_\pm(\theta, t) = \mathrm{Re}[\hat{\eta}_\pm \exp(\mathrm{i}k\theta - \mathrm{i}\sigma t)] \quad (k = 1, 2, 3, \ldots) \tag{3.4}$$

to the outer and inner edges of the ring, respectively, linearizing the equations of motion and solving a two-by-two determinant for the eigenvalue σ. The result is

$$\sigma = \pm\tfrac{1}{2}\omega\left(\left[1 - \tfrac{1}{2}k\left(\left(1 - \frac{a^2}{b^2}\right) - \Lambda\left((1-\exp(-a^2/r_0^2)) - \frac{a^2}{b^2}(1-\exp(-b^2/r_0^2))\right)\right)\right]^2 - \left(\frac{a}{b}\right)^{2k}\right)^{1/2}. \tag{3.5}$$

The expression for the disturbance (3.4) shows that the ring is stable provided σ is purely real. Introducing the dimensionless quantities

$$\hat{\omega} = \frac{\omega}{\omega_0}, \quad \hat{\sigma} = \frac{\sigma}{\omega_0}, \quad \hat{a} = \frac{a}{r_0}, \quad \hat{b} = \frac{b}{r_0}, \tag{3.6}$$

(3.5) becomes

$$\hat{\sigma} = \pm\tfrac{1}{2}\hat{\omega}\left(\left[1 - \tfrac{1}{2}k\left(\left(1 - \frac{\hat{a}^2}{\hat{b}^2}\right) - \Lambda\left((1-\exp(-\hat{a}^2)) - \frac{\hat{a}^2}{\hat{b}^2}(1-\exp(-\hat{b}^2))\right)\right)\right]^2 - \left(\frac{\hat{a}}{\hat{b}}\right)^{2k}\right)^{1/2}. \tag{3.7}$$

and $\Lambda = 1/(\hat{a}^2\hat{\omega})$. Figure 8 shows contours of $\mathrm{Im}(\sigma)$ in the $(\hat{k}, \hat{a})$-plane for a strip width $\hat{b} - \hat{a} = 0.05$ and strip vorticity of $\hat{\omega} = 1, 0.5, 0.25$. The contour plots in figure 8 show that the adverse shear generated by the Gaussian vortex is never sufficient to completely stabilize the strip if $\hat{\omega} = 1$ or $\hat{\omega} = 0.5$; however, when $\hat{\omega} = 0.25$ there is a fairly large band of stable positions $a = (0.6, 2.3)$. Thus we conclude that the adverse shear generated by a Gaussian vortex can only stabilize a weak circular filament at a narrow range of distances near the edge of the vortex. Filaments too far or too close are still unstable. Note, however, that Dritschel (1989) found that true nonlinear stability requires less adverse shear than suggested by the linear stability analysis. Thus the results presented here should be treated as conservative estimates of the stability of the filament.

Our results are consistent with those of Dritschel (1989) for the case of a central point vortex or a vortex patch: sufficient adverse shear can stabilize a circular filament. The major differences are due to the fact that Dritschel could not consider filaments within the vortex core, and that the smooth variation of shear in a Gaussian vortex leads to a more complicated stability pattern. In particular, there is an additional region of instability at the centre of the vortex.

The results of this linear stability analysis have been confirmed by a fully nonlinear DNS with initial conditions of a circular filament around a Gaussian vortex. These simulations show that filaments placed in the core of the vortex quickly become unstable. The instability starts as a small-scale perturbation that grows and eventually

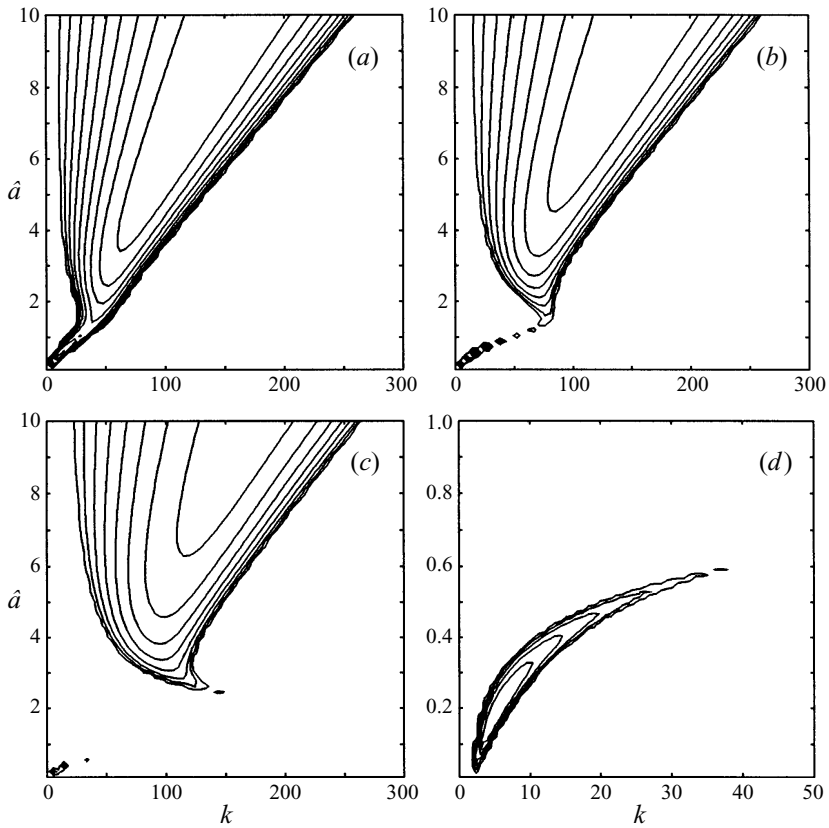

FIGURE 8. Contours of unstable phase space for a circular filament of width 0.05 around a Gaussian vortex of unit size and maximum vorticity. The contours of $\mathrm{Im}(\sigma)$ are plotted, k is the wavenumber of the perturbation and $\hat{a}$ is the distance from the centre of the vortex. 10 contours are plotted between zero and the maximum of $\mathrm{Im}(\sigma)$. (*a*) Vorticity of filament $\hat{\omega} = 1.0$, (*b*) $\hat{\omega} = 0.5$, (*c*) $\hat{\omega} = 0.25$, (*d*) $\hat{\omega} = 0.25$, closeup.

creates four new vortices along the circle at the initial radius of the filament. Weak filaments at the edge of the vortex are stable. These results show that neglecting the interaction between the strip and the filament is justified in the above analysis.

We have found an explanation for the stability of the weak filaments at the edge of the vortex, but the DNS shows that all the filaments created during the merger are stable, even those in the vortex core (see figure 1). We will show that this stability is due to straining of the filament by the vortex.

3.2. *Straining*

Dritschel *et al.* (1991) demonstrated that even a small amount of straining along the length of a vorticity filament can stabilize it. Since adverse shear cannot stabilize the filaments in the vortex core, straining may be the stabilizing effect. At this point it is important to note that the filaments created during the merger are not in fact circular (although the weak filaments at the vortex edge are close to circular), but are spirals that are constantly strained by the rotation of the vortex. This straining is especially pronounced in the core region of the vortex. Is this straining likely to be strong enough to stabilize the filaments?

For flows with continuous vorticity the strain rate γ and shearing rate $1/2\Lambda$ may

be computed from the formulae

$$\gamma = \hat{\boldsymbol{t}} \cdot \nabla \boldsymbol{u} \cdot \hat{\boldsymbol{t}}, \tag{3.8a}$$

$$\tfrac{1}{2}\Lambda = \hat{\boldsymbol{n}} \cdot \nabla \boldsymbol{u} \cdot \hat{\boldsymbol{t}}, \tag{3.8b}$$

where $\nabla \boldsymbol{u}$ is the velocity gradient tensor, $\hat{\boldsymbol{n}} = \nabla\omega/|\nabla\omega|$ is the unit vector parallel to the vorticity gradient and $\hat{\boldsymbol{t}} = -\hat{\boldsymbol{e}}_z \times \hat{\boldsymbol{n}}$ is a vector which points along the contours of vorticity and has larger vorticity on the right. By calculating γ/ω_f and $(1/2\Lambda)/\omega_f$, where ω_f is the vorticity in the filament, one can estimate whether the straining is sufficient to stabilize the filament.

We have seen that the shear actually destabilizes the filament in the vortex core, so we need only calculate the straining γ. In particular, we should calculate the straining along the spiral created by placing a strip of vorticity across the centre of a Gaussian vortex (we treat the vorticity as passive). The strain along the spiral filament is

$$\gamma = \frac{\mathrm{d}u_S}{\mathrm{d}S} = \frac{\partial u_S}{\partial r}\frac{\partial r}{\partial S} = -u'(r)r\frac{\partial \theta}{\partial S}\frac{\partial r}{\partial S} = -ru'(r)\frac{\partial \theta}{\partial r}\left(\frac{\partial r}{\partial S}\right)^2, \tag{3.9}$$

where the prime denotes differentiation with respect to r, u_S is the velocity component along the arclength of the spiral, $\partial/\partial S$ is the derivative along this arclength and $u(r)$ is the velocity component of the Gaussian vortex in the $\hat{\boldsymbol{\theta}}$-direction. But,

$$\frac{\partial r}{\partial S} = \left[1 - r^2\left(\frac{\partial \theta}{\partial S}\right)^2\right]^{1/2} = \left[1 + r^2\left(\frac{\partial \theta}{\partial r}\right)^2\right]^{-1/2},$$

and $\theta = (u(r)/r)t$, thus

$$\frac{\partial \theta}{\partial r} = \frac{t}{r^2}\left(ru'(r) - u(r)\right),$$

and therefore

$$\frac{\partial r}{\partial S} = \left[1 + \frac{t^2}{r^2}(ru'(r) - u(r))^2\right]^{-1/2}. \tag{3.10}$$

Combining (3.9) and (3.10) we find that the strain rate along a spiral in a Gaussian vortex is

$$\gamma = \frac{-(t/r)u'(r)(ru'(r) - u(r))}{1 + (t^2/r^2)(ru'(r) - u(r))^2} \tag{3.11}$$

where $u(r) = \Gamma/(2\pi r)(1 - \exp(-r^2/4))$ for the Gaussian vortex $\omega(r) = \Gamma/\pi \exp(-r^2/4)$.

Plots of the strain rate generated by the Gaussian vortex used in the DNS for spirals with varying numbers of turns are shown in figure 9(b), it shows that the peak strain rate grows and moves to smaller radii as time increases. Dritschel *et al.* (1991) demonstrated that a strain rate of $\gamma/\omega > 0.25$ completely removes all instabilities, and thus the Gaussian spiral straining should be strong enough to stabilize all filaments in the core region (since $\omega_f \leqslant \omega = \Gamma/\pi$).

Besides its stabilizing effect, the spiral straining also lengthens the filament, which means its width must decrease proportionally by conservation of vorticity of material surfaces. When the filaments are thin enough viscosity becomes dominant and they diffuse away. Calculations show that this thinning process is extremely rapid in the vortex core. Thus, spiral straining first stabilizes and then removes filaments from the vortex core. This picture is consistent with the results of the DNS (see figure 1).

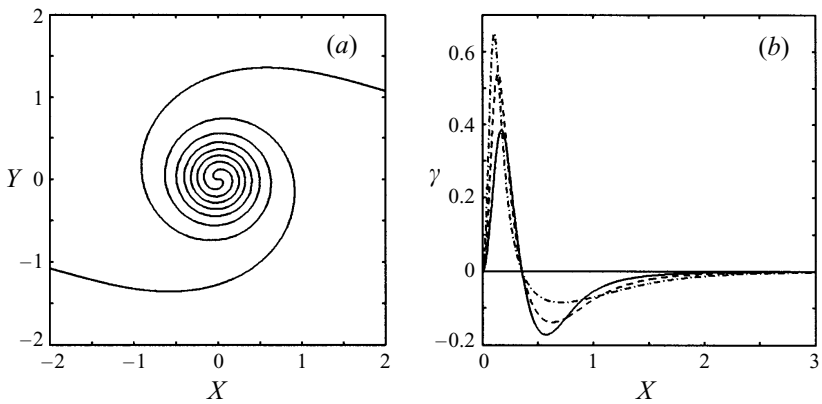

FIGURE 9. (*a*) A four-turn spiral created by a Gaussian vortex. (*b*) Strain rates along the spiral created by the DNS Gaussian vortex $\omega(r) = \pi \exp(-r^2\pi^2)$ with —, 2; – – –, 4; – · –, 8 turns (number of turns $N = t/(2\pi r_0^2/\Gamma)$ where r_0 is the radius of the vortex and Γ is its circulation).

4. Vortex with filaments in weak external strain

4.1. *Asymptotic calculation*

In the previous Section we showed that the filaments created during the merger of two vortices are stabilized by the new approximately Gaussian vortex that is formed. The filaments in the vortex core are stabilized and then dissipated by spiral straining, but the approximately circular filaments at the edge of the vortex are stabilized by adverse shear and exist for a relatively long time. The question we now address is how these stable filaments at the edge of the vortex affect its subsequent interactions. The effect of distant vortices is essentially a weak irrotational strain. In this section we follow the method of Ting & Tung (1966) and Jiménez *et al.* (1996) to calculate how the presence of a vorticity filament changes the deformation of a Gaussian vortex in response to weak irrotational strain. The degree of sensitivity to this weak straining determines how robust the vortices are, and whether they undergo merging interactions. Thus this response is a major factor controlling the vortex interactions which are responsible for the energy cascade and decay of two-dimensional turbulence.

Following Jiménez *et al.* (1996) we take a two-dimensional vortex of circulation Γ, subject to a constant uniform strain $s(x, -y)$. The velocity of the vortex and of the strain are comparable at a distance of order $R_s = (\Gamma/s)^{1/2}$, while the vortex size at a characteristic time $O(s^{-1})$ is of order $R_v = (\nu/s)^{1/2}$. Its characteristic vorticity is then $\omega_c = \Gamma/R_v^2$. We consider the weakly perturbed limit where

$$\epsilon = \frac{\nu}{\Gamma} = \frac{s}{\omega_c} = \left(\frac{R_v}{R_s}\right)^2 \ll 1. \tag{4.1}$$

When length is normalized by R_s and time by s^{-1}, the vorticity equation becomes

$$\frac{\partial \omega}{\partial t} - J(\psi, \omega) = \epsilon \nabla^2 \omega, \quad \omega = -\nabla^2 \psi \tag{4.2}$$

where $\psi \sim xy$ at infinity. Choosing inner variables

$$(\hat{x}, \hat{y}) = \epsilon^{-1/2}(x, y), \quad \hat{t} = t, \quad \hat{\psi} = \psi, \tag{4.3}$$

the vorticity equation becomes

$$J(\hat{\psi}, \hat{\omega}) = \epsilon \left(\frac{\partial \hat{\omega}}{\partial \hat{t}} - \nabla^2 \hat{\omega} \right). \tag{4.4}$$

The zeroth-order, or basic, solution is

$$J(\hat{\psi}, \hat{\omega}) = 0, \quad \hat{\omega}_0 = \hat{\omega}_0(\hat{\psi}_0), \tag{4.5}$$

where we assume the perturbation expansion $\hat{\omega} = \hat{\omega}_0 + \epsilon \hat{\omega}_1 + \ldots$, and a similar expansion for $\hat{\psi}$. Note that we will assume an axisymmetric basic solution.

The equation for the first-order perturbation is

$$J(\hat{\psi}_0, \hat{\omega}_1) + J(\hat{\psi}_1, \hat{\omega}_0) = \frac{1}{\hat{r}} \frac{\partial}{\partial \theta} \left(\hat{\omega}_1 \frac{\hat{\psi}_0}{\partial \hat{r}} - \hat{\psi}_1 \frac{\hat{\omega}_0}{\partial \hat{r}} \right). \tag{4.6}$$

If the above equation is averaged over all angles we obtain a compatibility condition that defines the basic solution

$$\frac{\partial \hat{\omega}_0}{\partial \hat{t}} - \hat{\nabla}^2 \hat{\omega}_0 = 0. \tag{4.7}$$

Substituting the compatibility equation (4.7) into the first-order perturbation equation (4.6) we get the equation defining the first-order solution

$$J(\hat{\psi}_0, \hat{\omega}_1) + J(\hat{\psi}_1, \hat{\omega}_0) = 0. \tag{4.8}$$

The directional and radial dependences can be separated to give the equation

$$\hat{\psi}_1 = 2 \left(\tfrac{1}{4} \hat{r}^2 - f(\hat{r}, \hat{t}) \right) \sin 2\theta, \tag{4.9}$$

where $f(\hat{r}, \hat{t})$ satisfies the boundary value problem

$$f'' + \frac{1}{\hat{r}} f' - \frac{4}{\hat{r}^2} f = \left(\tfrac{1}{4} \hat{r}^2 - f \right) \frac{\hat{\omega}_0'}{\hat{\psi}_0'}, \tag{4.10a}$$

$$f = O(\hat{r}^2) \quad \text{as} \quad \hat{r} \to 0, \qquad f = O(\hat{r}^{-2}) \quad \text{as} \quad \hat{r} \to \infty, \tag{4.10b}$$

where the prime denotes differentiation with respect to $\hat{r}$. Up until this point the derivation has exactly followed Jiménez *et al.* (1996), the only difference being that we have not used the self-similarity variable $\chi = \hat{r}/\hat{t}^{1/2}$ (since in our case the basic solution is not self-similar).

Jiménez *et al.* (1996) consider the basic solution which corresponds to a point vortex at $t = 0$,

$$\hat{\omega}_0(r, t) = \frac{1}{4\pi t} \exp(-\hat{r}^2/4\hat{t}), \tag{4.11}$$

which is a Gaussian vortex that spreads self-similarly as time increases ('Lamb's vortex'). To the diffusing point vortex we now add a diffusing ring vortex: the vortex one obtains when vorticity initially concentrated on a circle is allowed to diffuse. This ring vortex models the approximately circular vorticity filaments at the edge of the Gaussian vortex created by the merger. Note that the circulation Γ used for the normalization is the circulation of the Lamb's vortex alone. The addition of a ring vortex slightly decreases the region where irrotational strain dominates, but this does not affect the validity of the first-order asymptotic analysis.

In cylindrical coordinates the distribution of vorticity at any time t can be found

from its distribution at $t = 0$ via the formula

$$\omega(r,t) = \frac{1}{2\nu t}\int_0^\infty \exp(-(r^2+s^2))I_0\left(\frac{rs}{2\nu t}\right) s\omega(s,0)\,\mathrm{d}s, \tag{4.12}$$

where $I_0(x)$ is the zeroth-order modified Bessel function, and $\omega(r,0)$ is the vorticity distribution at $t = 0$ (Carslaw & Jaeger 1959). If sources of strength $\Gamma/2\pi\,\mathrm{d}\theta$ are evenly distributed around a circle of radius R (4.12) gives the vorticity distribution at time $\hat{t}$ as

$$\hat{\omega}(\hat{r},\hat{t}) = \frac{\Gamma}{4\pi\hat{t}}\exp[-(\hat{r}^2+R^2)/4\hat{t}]I_0\left(\frac{\hat{r}R}{2\hat{t}}\right), \tag{4.13}$$

where we have switched to normalized variables. Note that if $\hat{r}R/2\hat{t} \gg 1$ the above expression simplifies to

$$\hat{\omega}(\hat{r},\hat{t}) \approx \frac{\Gamma}{4\pi R(\pi\hat{t})^{1/2}}\exp[-(\hat{r}-R)^2/4\hat{t}]. \tag{4.14}$$

Because the vorticity filaments that form at the edge of a vortex during merging are effectively much younger than the vortex, for simplicity we will take the age of the Gaussian vortex to be unity and consider ring vortices of various ages. Thus the initial condition is a Lamb's vortex of age $1-\hat{t}$ (where $\hat{t}$ is the age of the ring vortex considered), plus a circle of vorticity. The total vorticity field at time $\hat{t}$ is therefore

$$\hat{\omega}(\hat{r},\hat{t}) = \frac{1}{4\pi}\left[\exp(-\hat{r}^2/4) + \frac{\Gamma}{\hat{t}}\exp[-(\hat{r}^2+R^2)/4\hat{t}]I_0\left(\frac{\hat{r}R}{2\hat{t}}\right)\right], \tag{4.15}$$

where the circulation of the Lamb's vortex is unity by the normalization, and Γ is the circulation of the ring vortex. For thin ring vortices $R/\hat{t} \gg 1$ (4.15) simplifies to

$$\hat{\omega}(\hat{r},\hat{t}) = \frac{1}{4\pi}(\exp(-\tfrac{1}{4}\hat{r}^2) + (\pi\hat{t})^{-1/2}\exp[-(\hat{r}-R)^2/4\hat{t}]). \tag{4.16}$$

The appropriate expression (4.15) or (4.16) can then be used to calculate the quantity $\hat{\omega}'/\hat{\psi}'$ in (4.10), where $\hat{\psi}'(\hat{r},\hat{t}) = -(1/\hat{r})\int_0^\infty s\hat{\omega}(s,\hat{t})\,\mathrm{d}s$. The function $f(\hat{r},\hat{t})$ is found by numerically solving the boundary value problem defined by (4.10).

Once the function $f(\hat{r},\hat{t})$ has been calculated, the ellipticity μ (which is a measure of the deformation of the streamlines or vorticity of the vortex) may be calculated from the formula

$$\mu = \frac{a-b}{a+b} = \epsilon\frac{|\hat{\psi}|_{max}}{\hat{r}|\hat{\psi}_0'|} + O(\epsilon^2) = \epsilon\frac{2(\frac{1}{4}\hat{r}^2 - f(\hat{r},\hat{t}))}{\hat{r}|\hat{\psi}_0'|}, \tag{4.17}$$

where a and b are respectively the major and minor axes of the ellipse.

Because it is difficult to define the age of a filament in the merging interaction, we consider ring vortices with a specified maximum vorticity $\hat{\omega}_{max}$ and circulation Γ relative to the Lamb's vortex, and calculate the age $\hat{t}$ accordingly. These quantities can be estimated from the DNS and compared with the results obtained here.

Figure 10(a) shows the ellipticity of the flow for high- and low-circulation rings, and no ring. At radii greater than $r = R$ the ring vortices always reduce the deformation, merely due to the additional shear associated with the filaments. However, inside the ring $r < R$ the ring vortices can either reduce *or* increase the deformation, depending on the strength and position of the ring. In order to quantify this dependence, in figure 10(b) the 'neutral curve' dividing reduced from increased deformations is plotted in the (Γ, R)-plane for three relative maximum vorticities $\hat{\omega}_{max} = 1, 0.5, 0.25$.

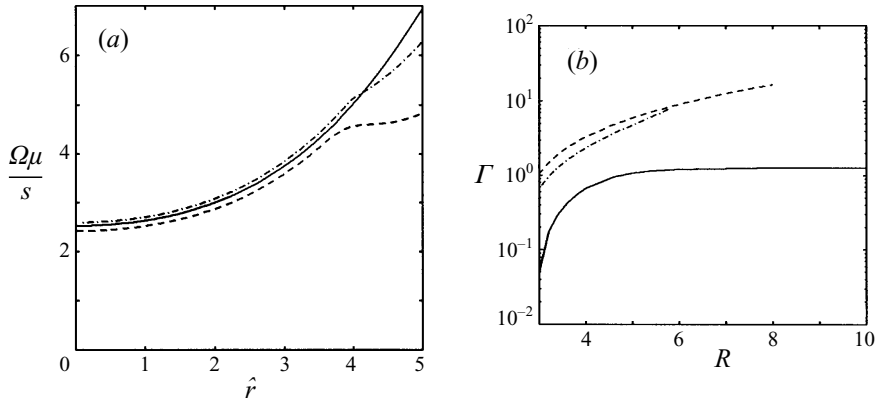

FIGURE 10. Effect of the ring vortex on the deformation of vortex core. (*a*) Ellipticity of the flow μ/ϵ as a function of radius r: —, no ring vortex; – – –, $\Gamma = 1$, $R = 4$, $\hat{\omega}_{max} = 1$; – · –, $\Gamma = 0.25$, $R = 4$, $\hat{\omega}_{max} = 1$. (*b*) Neutral deformation curve: below the curve the ring vortex reduces vortex core deformation, above it the ring vortex increases vortex core deformation: —, $\hat{\omega}_{max} = 1$; – – –, $\hat{\omega}_{max} = 0.5$; – · –, $\hat{\omega}_{max} = 0.25$.

The deformation was also calculated for several vortices with the same $\hat{\omega}_{max}$, but it was found that the total circulation is the only significant parameter. Three main qualitative conclusions may be drawn. The ring vortex reduces the deformation if: the ring is close enough to the vortex core, if its maximum vorticity is large enough compared to the central vortex, and if its circulation is large enough compared to the central vortex. Otherwise the vortex ring slightly increases deformation inside the ring $r < R$.

In the DNS the maximum possible circulation in the filaments at the edge of the vortex core is roughly equal to the circulation of the vortex core, and the maximum vorticity of the filaments is at most equal to the maximum vorticity of the core. Judging from figure 10(*b*), the filaments at the edge of the vortex core may slightly increase the deformation of the core compared to the case of no filaments. However, the kinks in the vortex core are in fact decayed filaments and these filaments may have a large circulation compared to the Lamb's vortex core. For example, a ring with $\Gamma = 4$, $R = 2$, $\hat{\omega}_{max} = 0.5$ produces a kink very similar to that seen in figure 2(*a*) at $t = 10$ and reduces the deformation by roughly 8%. Thus, the kinks in the core could significantly reduce the deformation due to distant vortices compared to the deformation of a Lamb's vortex alone.

There is also the question of how quickly the maximum vorticity of the ring vortex decays, and hence how long it has a significant effect on the deformation of the vortex core. Equation (4.14) shows that at small times $\hat{t} \ll R^2/4$ the ring decays slowly like $\hat{t}^{-1/2}$, whereas at longer times $\hat{t} \gg R^2/4$ the ring has diffused to form a single peak at the centre which decays quickly like $\hat{t}^{-1}$ (as for the Lamb's vortex). Between these two ranges is a transition range at $\hat{t} \sim R^2/4$ during which the maximum vorticity remains approximately constant. Adding several rings increases this 'quasi-equilibrium' transition period roughly proportionally to the number of rings. Physically, this is because the diffusing vorticity fills the gaps between the rings and is effectively not diffusing away. A longer transition period also means that the maximum vorticity is much higher than in the one-ring case once the $\hat{t}^{-1}$ range is reached. Thus, a sequence of ring vortices (or approximately circular spiral vortices) may alter the deformation of the vortex core for a significant period of time.

4.2. *Numerical calculation*

In the previous subsection we made a first-order asymptotic calculation of the effect of weak external strain on a Lamb's vortex surrounded by a ring vortex. This calculation indicates that the ring usually reduces the effect of external strain, although if the ring is weak and outside the vortex core it may have the opposite effect. We now present the results of a DNS to check the previous analytical results in a slightly more realistic situation.

The strain is produced by an array of two positive Lamb's vortices at $(\pi/2, \pi/2)$, $(3\pi/2, 3\pi/2)$ and two negative Lamb's vortices at $(\pi/2, 3\pi/2), (3\pi/2, \pi/2)$ in a square domain of size 2π. These vortices have a circulation of magnitude $|\Gamma_S| = 1/8$ and initial radius $r_0 = 1/(4\pi)$, and produce an approximately uniform strain of strength $s = 4\Gamma_s/\pi^3 + O((r/\pi)^4)$ near (π, π). We place another Lamb's vortex of the same size at (π, π) with circulation $\Gamma = 1/(4\pi^2)$. For these initial conditions the size of the 'cat's eye' where the asymptotic calculation should be valid is $R_s = 1/2$, and the ratio of the external strain to the maximum vorticity in the strained vortex is $1/(8\pi^2) \ll 1$, which shows that the external strain is indeed weak.

We consider three cases: no ring, a 'shielding' ring ($R = 3/2r_0$, $\Gamma_r = \Gamma$, ω_{max} is equal to ω_{max} of the central vortex), and an 'anti-shielding' ring ($R = 4r_0$, $\Gamma_r = 1/2\Gamma$, ω_{max} is half ω_{max} of the central vortex). All simulations are performed on a $1\,024^2$ grid with Newtonian viscosity $\nu = 5.0 \times 10^{-5}$ and are run until $t = 80$. The results of the simulations are shown in figure 11.

Figure 11(*b*) clearly shows that the shielding ring vortex reduces the deformation of the central Lamb's vortex, while figure 11(*c*) shows that the anti-shielding ring vortex has little effect. The quantitative results in figure 11(*d*) show the strong reduction in ellipticity produced by the shielding vortex inside the ring vortex. The anti-shielding vortex does in fact slightly increase the ellipticity near the centre of the Lamb's vortex, but slightly reduces the ellipticity at larger radii. Note that these effects are still significant at $t = 80$ even though figure 11(*a*) shows that by this time the rings have diffused into the vorticity profile of the Lamb's vortex. Figure 11(*d*) also confirms that the first-order asymptotic calculation predicts the ellipticity reasonably accurately in all three cases.

These results suggest that filaments in the vortex core may significantly reduce the deformation caused by weak strain, even at long times when the filaments have blended into the vortex core. (Note that figure 10*b* shows that intense filaments closer than about $3r_0$ should always be shielding, even for very small relative circulations.) Weaker vorticity filaments outside the vortex core may slightly increase the deformation very close to the centre of the vortex, and slightly reduce the deformation further away. However, both changes are very small and the effect of weak filaments outside the vortex core is probably negligible. The main effect of the filaments created during the vortex merger is thus to decrease the deformation caused by weak external strain and hence stabilize the new vortex.

4.3. *Physical explanation*

The shielding is in fact due to two different effects, which act in different regions at different times. Outside the ring ($r \geqslant R$), and at long times when the ring vorticity has diffused to the centre, the effect of external strain is reduced simply because the velocity gradient produced by the ring adds to that produced by the Lamb's vortex. The combination of the ring and the Lamb's vortex is essentially equivalent to a single, stronger vortex.

However, at short and intermediate times the ring vorticity at $r < R$ is still negligible

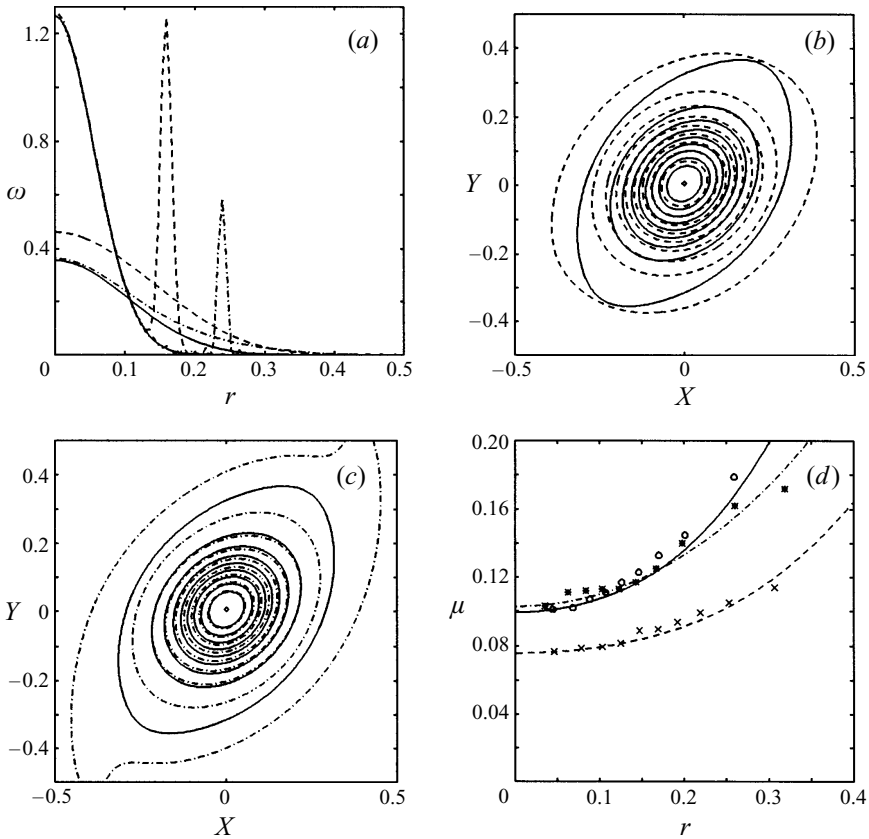

FIGURE 11. DNS calculation of the effect of weak external strain on a Lamb's vortex with and without ring vortices. In all figures: —, no ring vortex; – – –, 'shielding' ring vortex, –·–, 'anti-shielding' ring vortex. Note that in the contour plots 10 equally spaced contours are plotted between $(\omega_{max}/100, \omega_{max})$, which means contours for different cases are not necessarily at the same level. (*a*) Cross-section of vorticity field at $t = 0$ (initially upper curves) and $t = 80$ (lower curves). (*b*) Vorticity contours, comparison of no ring vortex and shielding ring vortex cases. (*c*) Vorticity contours, comparison of no ring vortex and anti-shielding ring vortex cases. (*d*) Comparison of asymptotic calculations of ellipticity (lines) with numerical results (symbols: o, no ring; ×, shielding ring; *, anti-shielding ring) for the three cases. The asymptotic curves have been normalized by matching the amplitude of the asymptotic curve for no ring at $r = 0.05$ to the amplitude of the equivalent DNS point. Note the significant reduction of ellipticity in shielding case, and slight increase in ellipticity near $r = 0$ in anti-shielding case.

and the previous mechanism does not apply. In this case the shielding is due to the deformation of the ring caused by the external strain. The strain compresses the ring in one direction and stretches it in the other. The DNS shows that the ring becomes narrower and more intense in the compressed direction and wider and less intense in the stretched direction (this is shown in figure 12*a*). Before the deformation the velocity inside the ring (due to the ring) is insignificant ($u_\theta(r) \sim \Gamma_r/(2\pi\delta^2)\exp(-R^2/\delta^2)$, $r \ll \delta$, where δ is the width of the ring). However, the elliptical deformation breaks the symmetry of the ring, and significant velocity gradients appear inside it (see figure 12*a*).

Qualitatively, one may understand the resulting velocity profiles as follows. In the compressed direction the vorticity becomes more concentrated and intense. The limit

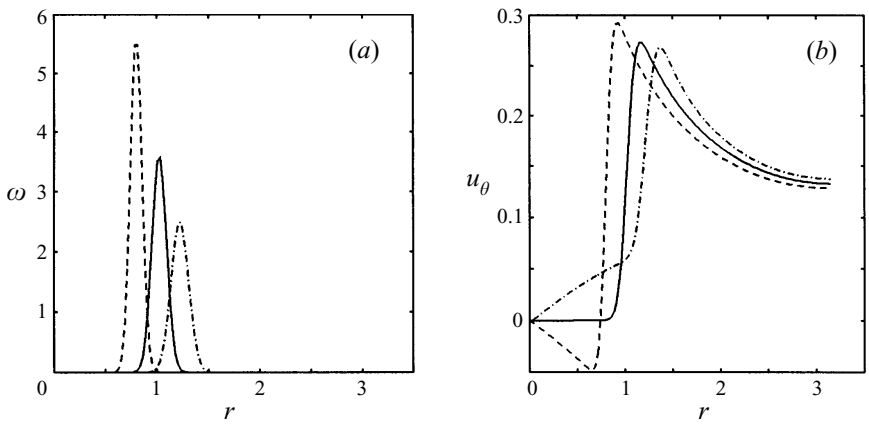

FIGURE 12. Model calculation of the velocity profile due to a circular and an elliptical ring vortex: —, circular ring vortex; – – –, elliptical ring vortex (compressed direction); – · –, elliptical ring vortex (stretched direction). (*a*) Vorticity cross-sections. (*b*) Velocity profiles, note the different gradients near the centre.

of this process is a pair of identical point vortices. The velocity profile of such vortices at $(\pm 1, 0)$ with circulation $\Gamma = 2\pi$ along the line separating them is

$$v(x,0) = \frac{-2x}{1-x^2} \sim -2x + O(x^3), \quad x \ll 1. \tag{4.18}$$

The velocity gradient $u'_\theta(r)$ of the Lamb's vortex is, however, positive and is increased by the external strain. Thus the negative velocity gradient induced by the elliptical ring vortex tends to oppose the action of the external strain. Now, in the stretched direction the vorticity spreads: the limit of this tendency is a vortex patch with a positive velocity gradient $u'_\theta(r)$. In the stretched direction the external strain tends to reduce the velocity gradient of the Lamb's vortex, thus the ring vortex opposes the action of the external strain in this direction as well. These velocity profiles are calculated numerically for a model elliptical ring vortex in figure 12(*b*). The previous argument does not, however, explain the small anti-shielding effect due to distant and weak ring vortices. This suggests that anti-shielding involves a more complex dynamical interaction between the central vortex and the ring.

5. Discussion and conclusions

In the first part of this paper we presented the results of a DNS of the merging of two identical positive Gaussian vortices pushed together by a weaker negative vortex. Identical DNS using both Newtonian and hyper-viscosity were performed and the results compared. The hyper-viscous simulation did not introduce any important spurious effects, but gave a good approximation to the equivalent high-Reynolds-number flow.

One of the main characteristics of the merging interaction is the formation of intense spiral filaments of vorticity. The filaments in the core blend quickly into the vortex profile, but leave 'kinks' in the vorticity profile that persist for long times. The filaments at the edge of the vortex remain well-defined for a longer time and thus the equilibrium configuration is a Gaussian vortex with kinks surrounded by a halo of approximately circular filaments at the edge. Roughly half the enstrophy goes into the new positive vortex, while the remainder goes into the filaments. We analysed

this interaction in both physical and Fourier space and found that the interaction generates power-law energy spectra typical of two-dimensional turbulence, and that these spectra are associated with the spiral vorticity filaments. The time-averaged energy spectra of the Newtonian and hyper-viscous simulations have power-law inertial ranges of k^{-4} and k^{-3} respectively. This spectrum should be representative of a two-dimensional turbulent flow containing many merging interactions at different stages. Thus, the k^{-4} and k^{-3} spectra might be interpreted as low- and high-Reynolds-number limits, respectively, for two-dimensional turbulence.

In the second part of the paper we considered the stability and effect of the vorticity filaments. We divided the vorticity field into filamentary and coherent parts using a novel wavelet packet technique. By restarting the simulations with the separated fields as new initial conditions we demonstrated that the coherent vortices do indeed stabilize the vorticity filaments.

A linear stability analysis showed that the adverse shear generated by a Gaussian vortex can only stabilize weak filaments in a fairly narrow band of distances at the edge of the vortex. We then calculated the strain rate generated by a Gaussian vortex along the spiral created when a passive strip of vorticity winds round the vortex. A comparison of this strain rate with the calculations of Dritschel *et al.* (1991) showed that it should be strong enough to stabilize filaments in the vortex core. The rapid straining also thins the filaments which makes them diffuse rapidly. Thus, coherent vortices stabilize filaments by a combination of adverse shear at the edge of the vortex and spiral straining in the vortex core. In fully developed two-dimensional turbulence filaments are only created during vortex interactions, thus it is likely that most filaments in these flows are also stable.

Finally, we used the asymptotic method of Jiménez *et al.* (1996) to calculate the effect of a filamentary circular ring vortex at radius R on the deformation of a Lamb's (Gaussian) vortex in an external weak irrotational strain. We found that the deformation (measured by the ellipticity of the vorticity contours) is always reduced compared to the case with no ring in the region outside the ring ($r > R$), but may be either reduced or slightly increased inside the ring $r < R$. The deformation is reduced if the ring is close enough to the vortex core, and has a strong enough maximum vorticity and circulation compared to the Gaussian vortex. The filaments generated at the edge of the vortex during the merging interaction may slightly increase the deformation near the centre of the vortex, while the kinks in the vortex core (remnants of ring vortices) may significantly decrease the deformation. In general, any increase in deformation due to weak filaments should be insignificant; however, filaments in the vortex core may significantly reduce the deformation due to weak external strain and hence stabilize the vortex. The results of the first-order asymptotic calculation were confirmed by performing a DNS of a Lamb's vortex in the weak irrotational strain field produced by four other vortices. The first-order asymptotic predictions of vortex ellipticity as a function of radius agreed reasonably well with the DNS results for vortices with and without rings.

These results show that vorticity filaments, although passive, may alter the dynamics of a two-dimensional turbulent flow by changing the response of a vortex to the strain of other vortices in the flow. This change in response may in turn modify such vortex characteristics as the minimum approach for merger and robustness.

Vorticity filaments may also have another important role: that of reducing entropy. Overall, entropy must increase during the merging interaction, but the end product of the interaction is a single coherent vortex. This structure clearly has a low entropy. However, vorticity filaments are ejected from the merging vortices and these filaments

then diffuse smoothly (since they are stable) which greatly increases the entropy. (In the merging interaction that we examined roughly half the enstrophy is dissipated in the form of filaments.) Thus, the coherent structures eject entropy (in the form of filaments) physically far from themselves in order to reduce their own entropy. The filaments serve a sort of 'house-cleaning' role in turbulence by physically separating the entropy-decreasing (coherent vortices) and the entropy-increasing (vorticity filaments) parts of the flow. The inhomogeneity in space of viscous dissipation (and diffusion of vorticity) is essential for, and created by, the coherent vortical structures of turbulence.

In summary, we have examined all stages in the 'life' of a vorticity filament: creation through vortex merger, stabilization by the new vortex, effect on subsequent vortex interactions, viscous diffusion and decay. The results help us to understand the role and properties of vorticity filaments in two-dimensional turbulence and may also explain more general properties such as the development of energy spectra, the robustness and nearly circular form of coherent vortices and the fact that filaments in two-dimensional turbulence show little sign of instability.

This research was supported by the Training and Mobility of Researchers programme of the EU under contract ERBFMBICT950365. The computations were performed on the Cray C98 of IDRIS under contract number 950317. We are grateful for the helpful comments of many colleagues and in particular for the advice of David Dritschel, and to Eric Goirand for kindly providing the wavelet packet software.

Appendix A. Vortex terminology

The notion of a filament of vorticity in two-dimensional turbulence (Dritschel *et al.* 1991; Gilbert 1988) is different from that of a filament of vorticity in three-dimensional turbulence (Douady, Couder & Brachet 1991; Moffatt, Kida & Ohkitani 1994; Jiménez *et al.* 1993). In two-dimensional turbulence the 'filaments' are one-dimensional structures which therefore cannot have internal organization, while in three-dimensional turbulence the 'filaments' are two-dimensional structures which may have internal organization (e.g. Schwartz 1990). During the preparation of this article, which deals with two-dimensional turbulence, we considered replacing the term 'filament' by a new term, for example 'thread', in order to clarify the terminology. Finally, however, we decided that it is preferable to retain the term vorticity 'filament' for the two-dimensional case, and we propose that the term vorticity 'tube' be adopted for the three-dimensional case.

We therefore propose that the term 'filament' be reserved to characterize the one-dimensional vorticity structures in the background flow which result from the interactions of coherent structures. Such filaments are generic in two-dimensional flows, but may also occur in three-dimensional flows. We propose that the term vorticity 'tube' be used to characterize the two-dimensional coherent vortices observed in three-dimensional turbulence. It is important that vorticity tubes and vorticity filaments are clearly distinguished because they are different types of structures: vorticity tubes are relatively long-lived concentrations of vorticity which are dynamically active, while vorticity filaments are transitory and largely passive. Moreover, it seems to us that this clarification of the taxonomy of turbulence must be taken seriously because there is at present a profusion of different terminologies (worms, 'vermisseaux', ribs, sinews ...) that tend to confuse and may prevent a better theoretical understanding of the nature and role of the coherent structures that have been observed in turbulence.

Appendix B. Statistical interpretation

One should be very cautious when attempting to make a statistical interpretation of energy spectra obtained from numerical simulations of turbulent flows. We believe that a statistical interpretation is hardly relevant for such simulations because the energy spectra are obtained from only one realization of a flow computed for a periodic domain, or for a finite domain with boundary conditions.

A statistical interpretation of the energy spectra relies on the hypothesis that turbulence, namely the Navier–Stokes dynamics in the limit of very large Reynolds numbers, is a stationary and ergodic random process described by random variables having definite probability distributions. In general, these properties allow us to interchange averages over space and averages over time. Thus a space average over a single realization of a turbulent flow may be treated as equivalent to averaging many different realizations, provided that the spatial dimensions of the flow are much larger than its integral scale. In particular, Wiener–Khintchine's theorem, which states that the Fourier transform of one realization of a stationary and ergodic random process in $\mathfrak{R}^n$ is the same as the Fourier transform of the correlation function of this process, can then be used to relate energy spectra and correlations.

Unfortunately, numerical simulations never use an unbounded domain $\mathfrak{R}^n$, but are obliged to use a bounded domain with given boundary conditions, or a torus with periodic boundary conditions. Moreover, the cases studied in this paper are not stationary because there is no external forcing to compensate the dissipation of enstrophy and thus the flow is in a decaying regime. Finally, the ergodic hypothesis is probably not valid either because we consider a very special case derived from the three-point vortex system which, in the inviscid limit, converges to a single point in a finite time. In any case, even if the random process is ergodic, the realization of the flow we are studying has not had sufficient time to visit the entire phase-space of the two-dimensional Navier-Stokes attractor. These comments also apply to most numerical simulations of turbulence.

For all these reasons, we do not think that a statistical interpretation of the energy spectra is appropriate. We propose instead a geometrical interpretation, which relates the power-law behaviour of the energy spectra to the shape and spatial distribution of the most singular coherent structures produced by the nonlinear dynamics of the turbulent flow (Farge & Holschneider 1991; Farge *et al.* 1992).

REFERENCES

Aref, H. 1979 Motion of three vortices. *Phys. Fluids* **22**, 393–400.

Basdevant, C., Legras, B., Sadourny, R. & Béland, M. 1981 A study of barotropic model flows: intermittency, waves and predictability. *J. Atmos. Sci.* **38**, 2305–2326.

Batchelor, G. K. 1969 Computation of the energy spectrum in homogeneous two-dimensional turbulence. *Phys. Fluids* **12**, II-233–II-239.

Carslaw, H. S. & Jaeger, J. C. 1959 *Conduction of Heat in Solids*. Clarendon.

Douady, S., Couder, Y. & Brachet, M. 1991 Direct observation of the intermittency of intense vorticity filaments in turbulence. *Phys. Rev. Lett.* **67**, 983–986.

Dritschel, D. G. 1989 On the stabilization of a two-dimensional vortex strip by adverse shear. *J. Fluid Mech.* **206**, 193–221.

Dritschel, D. G., Haynes, P. H., Juckes, M. N. & Shepherd, T. G. 1991 The stability of a two-dimensional vorticity filament under uniform strain. *J. Fluid Mech.* **230**, 647–665.

Dritschel, D. G. & Waugh, D. W. 1992 Quantification of the inelastic interaction of unequal vortices in two-dimensional vortex dynamics. *Phys. Fluids* A **4**, 1737–1744.

Dritschel, D. G. & Zabusky, N. J. 1996 On the nature of vortex interactions and models in unforced nearly-inviscid two-dimensional turbulence. *Phys. Fluids* **8**, 1252–1256.

Farge, M., Goirand, E., Meyer, Y., Pascal, F. & Wickerhauser, M. V. 1992 Improved predictability of two-dimensional turbulent flows using wavelet packet compression. *Fluid Dyn. Res.* **10**, 229–250.

Farge, M. & Holschneider, M. 1991 Interpretation of two-dimensional turbulence energy spectrum in terms of quasi-singularity in some vortex cores. *Europhys. Lett.* **15**, 737–743.

Farge, M., Holschneider, M. & Colonna, J. F. 1990 Wavelet analysis of coherent structures in two-dimensional turbulent flows. In *Topological Fluid Mechanics* (ed. H. K. Moffatt & A. Tsinober). Cambridge University Press.

Farge, M., Holschneider, M. & Philipovitch, T. 1992 Formation et stabilité des structures cohérentes quasi singulières en turbulence bidimensionnelle. *C. R. Acad. Sci. Paris* **315** II, 1585–1592.

Fornberg, B. 1977 A numerical study of 2-D turbulence. *J. Comput. Phys.* **25**, 1–31.

Gilbert, A. D. 1988 Spiral structures and spectra in two-dimensional turbulence. *J. Fluid Mech.* **193**, 475–497.

Jiménez, J. 1994 Hyperviscous vortices. *J. Fluid Mech.* **279**, 169–176.

Jiménez, J., Moffatt, H. K. & Vasco, C. 1996 The structure of the vortices in freely decaying two-dimensional turbulence. *J. Fluid Mech.* **313**, 209–222.

Jiménez, J., Wray, A. A., Saffman, P. G. & Rogallo, R. S. 1993 The structure of intense vorticity in isotropic turbulence. *J. Fluid Mech.* **255**, 65–90.

Kraichnan, R. H. 1967 Inertial ranges of two-dimensional turbulence. *Phys. Fluids* **10**, 1417–1423.

Legras, B., Santangelo, P. & Benzi, R. 1988 High resolution numerical experiments for forced two-dimensional turbulence. *Europhys. Lett.* **5**, 37–42.

McWilliams, J. 1984 The emergence of isolated coherent vortices in turbulent flow. *J. Fluid Mech.* **146**, 2–43.

Marchioro, C. & Pulvirenti, M. 1994 *Mathematical Theory of Incompressible Nonviscous Fluids.* Springer.

Mariotti, A., Legras, B. & Dritschel, D. G. 1994 Vortex stripping and the erosion of coherent structures in two-dimensional flows. *Phys. Fluids* **6**, 3954–3962.

Moffatt, H. K., Kida, S. & Ohkitani, K. 1994 Stretched vortices – the sinews of turbulence; large-Reynolds-number asymptotics. *J. Fluid Mech* **259**, 241–264.

Nielsen, A. H., He, X., Rasmussen, J. J. & Bohr, T. 1996 Vortex merging and spectral cascade in two-dimensional flows. *Phys. Fluids* **8**, 2263–2265.

Novikov, E. A. & Sedov, Yu. B. 1979 Vortex collapse. *Sov. Phys. JETP* **50**(2), 297–301.

Saffman, P. G. 1971 On the spectrum and decay of random two-dimensional vorticity distributions at large Reynolds number. *Stud. Appl. Maths* **50**, 377–383.

Schwartz, K. W. 1990 Evidence for organized small-scale structure in fully developed turbulence. *Phys. Rev. Lett.* **64**, 415–418.

Ting, L. & Tung, C. 1965 Motion and decay of a vortex in a nonuniform stream. *Phys. Fluids* **8**, 1039–1059.

Vassilicos, J. C. & Hunt, J. C. R. 1991 Fractal dimensions and spectra of interfaces with application to turbulence. *Proc. R. Soc. Lond.* A **435**, 505–534.

Vosbeek, P. W. C., Geffen, J. H. G. M. van, Meleshko, V. V. & Heijst, G. J. F. van 1997 Collapse interactions of finite-sized two-dimensional vortices. Submitted to *Phys. Fluids.*

Waugh, D. W. 1992 The efficiency of symmetric vortex merger. *Phys. Fluids* A **4**, 1745–1758.

Yao, H. B., Zabusky, N. J. & Dritschel, D. G. 1995 High gradient phenomena in two-dimensional vortex interactions. *Phys. Fluids* **7**, 539–548.